

# Nonlinear Time-Series Analysis of Photoinduced Fluorescence Oscillation in a Water Dispersion of Colloidal Quantum Dots

Shinya Maenosono,\* Noriko Eiha, and Yukio Yamaguchi

Department of Chemical System Engineering, University of Tokyo, Hongo 7-3-1, Bunkyo-ku, Tokyo 113-8656, Japan

Received: October 24, 2002; In Final Form: January 15, 2003

We report on photoinduced fluorescence oscillation observed in a water dispersion of CdSe/ZnS core/shell quantum dots (QDs). The fluorescence intensity spontaneously oscillates under continuous excitation in a temperature-sensitive manner and emerges at 29–30 °C. The experimental results suggest that the fluorescence oscillation occurs only in the presence of QD aggregates. The oscillation is characterized by wavelet and nonlinear time-series analyses of the fluorescence intensity data at 30 °C. The results reveal self-similarity and nonlinearity, suggesting that the fluorescence oscillation is governed by nonlinear dynamics and is a special class of photoinduced chemical oscillation.

## 1. Introduction

Colloidal semiconductor quantum dots (QDs) exhibit interesting and potentially useful size-dependent photophysical properties based on quantum confinement effects and as such have attracted a great deal of attention in recent years.<sup>1–3</sup> Optical spectra can be precisely tuned by varying the QD size, and the ability to control the fluorescence spectrum and excite QDs of different sizes simultaneously using a single excitation source holds great potential for biological applications, offering advantages over conventional organic dyes.<sup>4</sup> Although recent advances in the synthesis of water-soluble highly luminescent QDs have made biological use feasible,<sup>4–6</sup> there remain several problems obstructing the use of QDs as biological labels. When employing QDs as a tag for single biomolecules, fluorescence blinking and spectral diffusion phenomena due to photoionization<sup>7</sup> would prevent ready identification of QDs during single-molecule tracing. The stability of dispersion under severe conditions such as low pH in lysosomes is an important consideration in the observation of intracellular distributions or metabolism dynamics using QDs. To improve the dispersion stability, various types of surface modification have been reported, and stable silica-coated QDs have recently been proposed.<sup>8</sup> However, the dependence of the optical properties of these stabilized QDs on pH and salt concentration remains unclear. As interaction between QDs and ions in the dispersant is expected, such phenomena should be given careful consideration when developing QDs as *in vivo* biolabels.

Here we report on photoinduced fluorescence oscillation observed in a water dispersion of CdSe/ZnS core/shell QDs. The fluorescence oscillation occurs spontaneously in a specific temperature range under continuous excitation, and the amplitude of oscillation gradually attenuates over time.

In general, the oscillatory behavior of chemical systems is well understood,<sup>9</sup> and extensive studies have been conducted in this area in order to clarify self-organization mechanisms.<sup>10</sup> For example, the chemically oscillating Belousov–Zhabotinsky (BZ) reaction is a well-known nonequilibrium system<sup>11</sup> in which

both simple oscillations and bistable and chaotic behavior can emerge in a closed system.<sup>12–14</sup> Photoinduced bifurcations in a well-stirred solution,<sup>15,16</sup> photoinduced formation of spatio-temporal patterns in an unstirred solution,<sup>17,18</sup> and photoinduced chaos<sup>19,20</sup> have also been reported.

If the fluorescence oscillation in a closed, unstirred QD–water system is similar to such chemical oscillation, the time series of fluorescence intensity will exhibit some nonlinearity. To examine whether this is the case, the present authors carried out nonlinear time-series analyses of fluorescence oscillation in a closed, unstirred QD–water system.

## 2. Experimental Section

**2.1. QD Synthesis and Sample Preparation.** Water-soluble CdSe/ZnS core/shell QDs were synthesized by the colloid chemical method.<sup>21,22</sup> Rapid injection of a mixture of dimethylcadmium and selenium into a hot tri-*n*-octylphosphine oxide (TOPO) matrix forms CdSe QDs capped with TOPO molecules. Monodisperse CdSe QDs with a mean diameter of 4.2 nm were separated from the matrix by antisolvent precipitation. The CdSe cores were then redispersed in a hot TOPO matrix, to which diethylzinc and hexamethyldisilathiane were added dropwise. TOPO molecules on the QD surface were then replaced with 11-mercaptopundecanoic acid (MUA) to give MUA-capped CdSe/ZnS core/shell QDs. The absorption and fluorescence peak wavelengths of as-prepared MUA-capped QDs were 530 and 558 nm, respectively. By redispersing the QDs in deionized water, a clear dispersion with no aggregation was obtained (as-prepared suspension), as observed by dynamic light scattering (DLS; LEZA-600S, Photol) measurements. QD suspension of 10 wt % solid was prepared and stored at 25 °C for about 1 month (ripened suspension). The ripened suspension was ultrasonicated for 20 min at room temperature and then diluted with deionized water to a QD concentration of 0.3 wt % immediately prior to use. This diluted suspension contained QD aggregates of 100 nm in size (confirmed by DLS), and had a pH of  $8.0 \pm 0.2$ . The fluorescence peak wavelength of the ripened QD suspension was 567 nm, which is slightly red-shifted from that of the as-prepared suspension presumably due to long-range energy transfer from smaller to larger dots in the

\* Corresponding author. Fax: +81-5841-7279. E-mail: shinya@chemsys.t.u-tokyo.ac.jp.

**TABLE 1: Details of Samples Used in Experiments**

no.	PL peak (nm)	pH	NaCl (mM)	mean diam of aggregates (nm)	conductivity ( $\mu\text{S}/\text{cm}$ )
1	567	8	0	97	38
2	567	8	1	263	195
3	567	8	10	<i>a</i>	1500
4	568	9	0	112	56
5	568	10	0	104	114
6	554	8	0	$\sim 40$	
7	584	8	0	$\sim 40$	

<sup>a</sup> Large aggregates (not measurable).

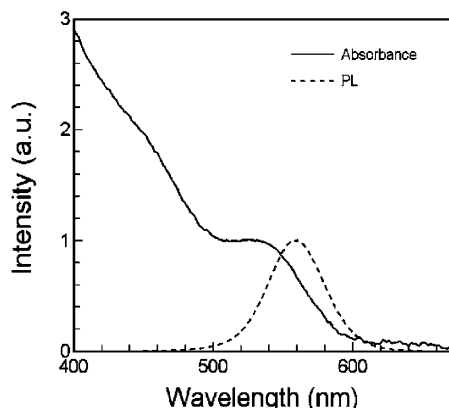


**Figure 1.** Absorption (solid line) and PL (dashed line) spectra of as-prepared QD suspension.

aggregates.<sup>23</sup> Five different samples of various pHs and salt concentrations were prepared by adding appropriate amounts of NaOH and NaCl. Additionally, we have synthesized two different MUA-capped CdSe/ZnS core/shell QDs of small and large core sizes to investigate the dependence of QD size on

the fluorescence properties. These QDs were synthesized at strictly the same conditions except for the core size and stored at 50 °C for 3 days. The absorption peak wavelengths of the small and large QD suspension were 538 and 550 nm, respectively (the fluorescence peaks were 554 and 584 nm, respectively). The conductivity of the suspension was measured using a digital conductivity meter. Details of all samples used in the experiments are summarized in Table 1.

**2.2. Fluorescence Intensity Measurements.** A 2 mL sample of the QD suspension was placed in a polystyrene cuvette set in a water-cooled holder of a fluorescence spectrophotometer (FP-6500, Jasco) for measurement of photoluminescence (PL) spectra and evolution of PL peak intensity. For progressive measurements, the QD suspension was continuously excited by monochromatic light (442 nm), and the PL intensity at the peak wavelength was recorded periodically. The cross-sectional area of the spectrophotometer light beam was 12 mm<sup>2</sup>, and the volume spanned by the beam was 126 mm<sup>3</sup> (6.3% of the total volume). The light spot was located 5 mm from the liquid–air interface, 11 mm from the bottom of the cuvette, and about 2 mm from the sides. The temperature, pH, and salt concentration dependences of the temporal variation in PL intensity were investigated at temperatures from 25 to 35 °C.

### 3. Theory

**3.1. Wavelet Transform.** Several methods may be employed to analyze transient signals, including short-time Fourier transformation, Wigner distribution, and wavelet transformation. As the wavelet transform is the most widely used in a number of fields,<sup>24</sup> the continuous wavelet transform is adopted in this study to extract the transient behavior from the time-series data of PL intensity. The wavelet transform of a function  $x(t)$  is given by

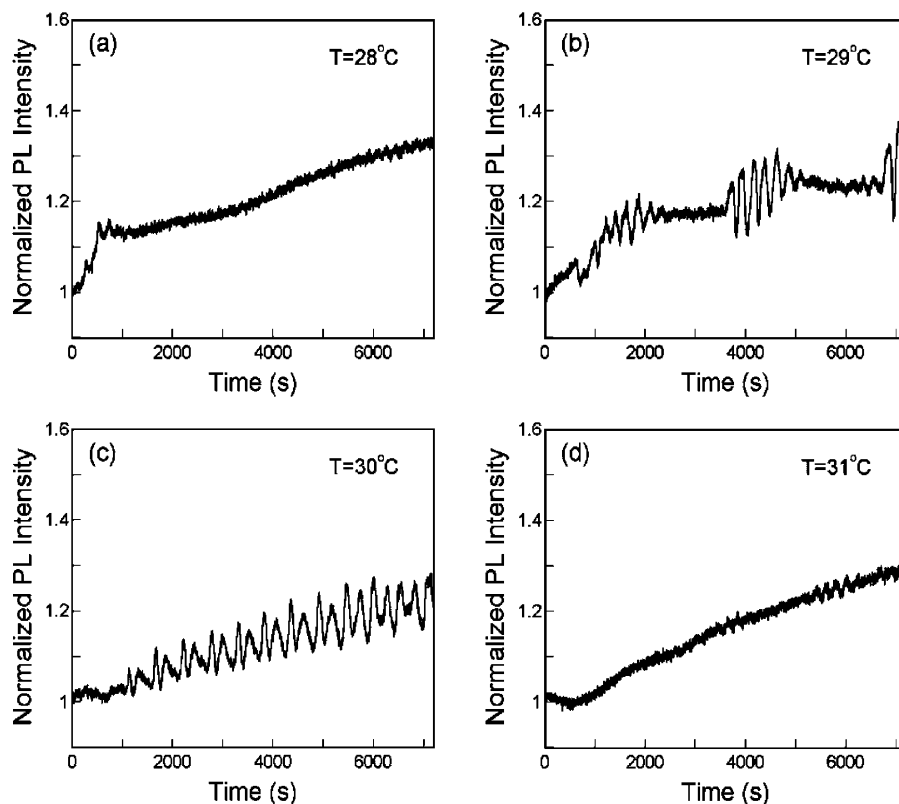


**Figure 2.** PL peak intensity normalized to the initial value plotted as a function of excitation time at temperatures of (a)  $T = 28$  °C, (b)  $T = 29$  °C, (c)  $T = 30$  °C, and (d)  $T = 31$  °C.

$$\Psi_{a,b} = \int_{-\infty}^{\infty} x(t) \psi_{a,b}(t) dt \quad (1)$$

where  $\psi_{a,b}(t)$  is a wavelet function defined as<sup>25</sup>

$$\psi_{a,b}(t) = \frac{1}{\sqrt{a}} \psi\left(\frac{t-b}{a}\right) \quad (2)$$

Here,  $\psi(t)$ ,  $a$ , and  $b$  are the mother wavelet, scale, and shift parameters, respectively. The mother wavelet  $\psi(t)$  must satisfy the following admissibility condition.

$$\int_{-\infty}^{\infty} \frac{|\hat{\psi}(\omega)|^2}{|\omega|} d\omega < \infty \quad (3)$$

where  $\hat{\psi}(\omega)$  denotes the Fourier transform of  $\psi(t)$ . The Gabor function was used for the mother wavelet, as follows.

$$\psi(t) = \pi^{-1/4} \xi^{1/2} \exp\left(-\frac{t^2}{2\xi^2} - i\omega_p t\right) \quad (4)$$

$$\hat{\psi}(\omega) = \pi^{-1/4} \xi^{-1/2} \exp\left[-\frac{(\omega - \omega_p)^2}{2\xi^2}\right] \quad (5)$$

Here,  $\omega_p$ ,  $2\xi = 2\omega_p/\gamma$ , and  $\gamma$  are the central frequency, half-value width of the window in the frequency domain, and the tuning parameter, respectively. By defining  $\Delta t$  and  $\pi/\Delta t$  as the sampling interval and the Nyquist frequency, the following parameters satisfy eq 3.<sup>26</sup>

$$a_p = 2^{p/4} \quad b_q = q\Delta t \quad \gamma = 5.336 \quad \omega_p = \sqrt{2}\pi/\Delta t \quad (6)$$

where  $p$  and  $q$  are the adjusting parameters. In applying eq 1 to the discrete time series, the integration period is limited to  $0 \leq t \leq N\Delta t$  and  $0 \leq p \leq 40$ , where  $N$  is the number of sampling points. Additionally, the condition  $0 \leq q \leq N/2$  should be satisfied.<sup>26</sup>

**3.2. Correlation Dimension.** The fractal dimension is one of the most important quantities in characterizing the fractality in dissipative dynamic systems. To extract the fractal dimension from a one-dimensional time series, it is necessary to reconstruct the geometry in phase space. Here, time-delayed phase-space reconstruction is employed to transform the one-dimensional time series  $x(t)$  to an  $m$ -dimensional delay vector  $y(n)$  via the relation

$$y(n) = (x(n\Delta t), x(n\Delta t - \tau), x(n\Delta t - 2\tau), \dots, x(n\Delta t - (m-1)\tau))' \quad (n = 1, \dots, N) \quad (7)$$

where the prime denotes a vector transposition, and  $m$  and  $\tau$  are the embedding dimension and time delay. Although the Hausdorff dimension  $D_H$  and information dimension  $D_I$  are the most natural indices for characterizing fractal sets mathematically and physically,<sup>27</sup> the correlation dimension  $D_2$ ,<sup>28</sup> a more powerful index for characterizing measured data and one that is commonly used to examine fractal geometry, is employed in this case. In this method, the self-similar property of an attractor is probed based on the scaling behavior of the following correlation sum.<sup>28</sup>

$$C(r, m) = \frac{1}{N_{\text{pairs}}} \sum_{j=m}^N \sum_{k < j} \Theta(r - |y(j) - y(k)|) \quad (8)$$

where  $r$  is the small radius of an  $m$ -dimensional ball in the phase space,  $N_{\text{pairs}} = (N - m + 1)^2/2$  is the number of pairs of points

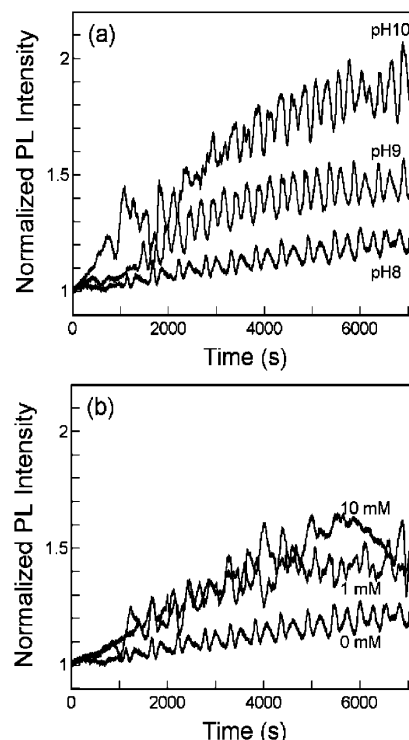


**Figure 3.** PL peak intensity normalized to the initial value plotted as a function of excitation time. (a) pH dependence on the oscillatory behavior. Lines of pH = 8, 9, and 10 correspond to the temporal variation of normalized PL intensity of samples 1, 4, and 5 (see Table 1). (b) NaCl concentration dependence. Lines of 0, 1, and 10 mM correspond to the time series of samples 1, 2, and 3 (see Table 1).

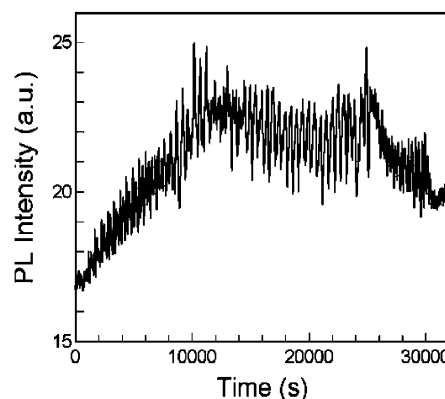


**Figure 4.** Complete set of normalized PL intensity data for  $T = 30$  °C (as shown in Figure 2c). The sampling interval was  $\Delta t = 2$  s, and the number of sampling points was  $N = 16\,000$ .

covered by the sums, and  $\Theta$  is the Heaviside step function. On sufficiently small length scales and when the embedding dimension  $m$  exceeds the box dimension of the attractor, there exists the scaling relation

$$C(r, m) \propto r^{D_2} \quad (9)$$

The correlation dimension  $D_2(r, m)$  can be readily determined as the slope of  $\ln C(r, m)$  versus  $\ln r$  in the scaling region. If  $D_2$  clearly plateaus over a wide range of length scales and for all embedding dimensions larger than a minimal dimension, the existence of common behavior is suggested and the dimension (the value of the plateau) for the system can be inferred.

**3.3. Surrogate Analysis.** The examination of surrogate data has been proposed by Theiler et al.<sup>29</sup> as a test of whether a time series exhibits nonlinearity, and has been widely applied

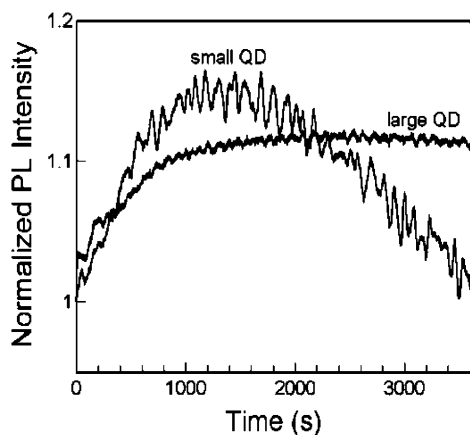


**Figure 5.** Temporal variations of normalized PL intensity of small and large MUA-capped CdSe/ZnS core/shell QDs (samples 6 and 7 in Table 1) for  $T = 30\text{ }^{\circ}\text{C}$ . The absorption peak wavelengths of the small and large QDs were 538 and 550 nm, respectively.

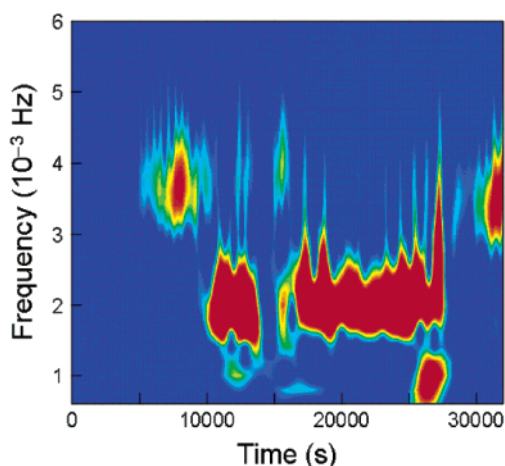


**Figure 6.** Scalogram of time series shown in Figure 4. Fundamental ( $\omega = 4 \times 10^{-3}\text{ Hz}$ ) and 1/2-subharmonic of the fundamental ( $\omega = 2 \times 10^{-3}\text{ Hz}$ ) frequencies can be clearly identified.

to real-world time series.<sup>30</sup> A null hypothesis is formulated, and if this hypothesis can be disproven by comparing results for the data to appropriate realizations of the null hypothesis, the data are considered to include a nonlinear component. Three particularly useful null hypotheses are that the data are (1) independent and identically distributed noise, (2) linearly filtered noise, and (3) a monotonic nonlinear transformation of linearly filtered noise. The three surrogate generation algorithms corresponding to each of these hypotheses are the (1) random shuffle, (2) phase randomized, and (3) amplitude adjusted Fourier transform (AAFT) algorithms.<sup>31</sup> In the case of the AAFT algorithm, convergence of the power spectrum has been reported to be poor, and improvements may be realized by iterating the surrogate generation algorithm.<sup>32</sup> This improved algorithm is the iterative AAFT (IAAFT) surrogate algorithm. In this paper, the IAAFT algorithm was employed with 10 surrogates generated for analysis.<sup>33</sup> If the correlation dimension  $D_2$  of the original data and that of the surrogate data are distinct, the null hypothesis can be rejected.

#### 4. Results and Discussion

Figure 1 shows the absorption and PL spectra of the as-prepared QD suspension. The QD suspension has typical absorption and PL spectra, exhibiting absorption peak blue shift in comparison to the bulk crystal. Figure 2 is a plot of the PL

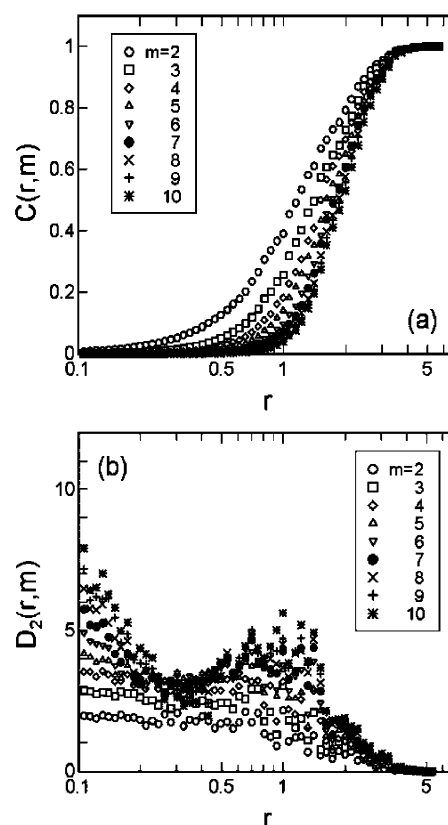


**Figure 7.** (a) Correlation sums  $C(r,m)$  and (b) correlation dimensions  $D_2(r,m)$  of the time series shown in Figure 4, calculated for all embedding dimensions ( $2 \leq m \leq 10$ ).

peak intensity as a function of excitation time at temperatures of (a)  $T = 28\text{ }^{\circ}\text{C}$ , (b)  $T = 29\text{ }^{\circ}\text{C}$ , (c)  $T = 30\text{ }^{\circ}\text{C}$ , and (d)  $T = 31\text{ }^{\circ}\text{C}$ . The PL intensity oscillates as the temperature increases through 29–30  $^{\circ}\text{C}$ , and the PL intensity increases monotonically over time at other temperatures. No oscillation was observed at either of the two end temperatures (25 and 35  $^{\circ}\text{C}$ ).

After storage in the dark, the enhanced PL intensity returned to the initial level. The reversibility of this phenomenon was confirmed by fully irradiating the cuvette with UV light and periodically recording the PL intensity using a fluorescence spectrophotometer to track PL recovery. Therefore, the PL enhancement observed at temperatures in the range  $25 \leq T \leq 35\text{ }^{\circ}\text{C}$  is probably due to some reversible photoreaction. One possibility is photoinduced surface passivation by water molecules during excitation.<sup>34</sup> This mechanism, however, does not explain the observed pH and salt concentration dependences as described later. Photoionization-induced PL enhancement is another possibility. This effect has been reported for a close-packed QD (TOPO-capped CdSe) film,<sup>35–37</sup> and has been suggested to be due electron trapping in the matrix and/or at the QD surfaces when a certain fraction of QDs in close-packed films is photoionized. This leads to the enhancement of total emission efficiency as a result of a decrease in the ionization probability of the remaining neutral QDs at higher electrostatic potential. The gradual PL enhancement in the QD–water system can be similarly explained by this hypothesis for electrostatic potential around QDs in a close-packed aggregate. QD aggregates of about 100 nm size were in fact observed by DLS, as shown in Table 1. We note that no change was observed in the QD suspension by visual inspection after the long-period irradiation; that is, there was no macroscopic precipitate in the bottom of the sample. This indicates that the QD aggregates are stable throughout the fluorescence measurement. This



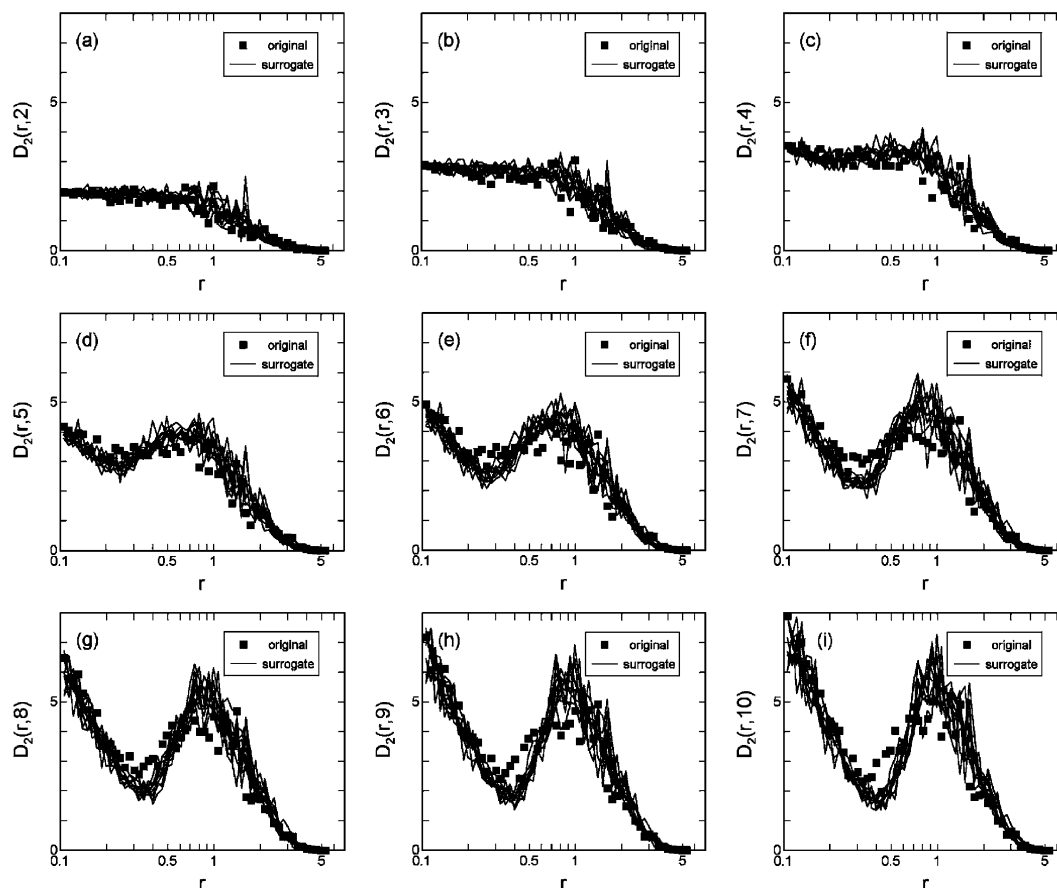


**Figure 8.** Correlation dimensions  $D_2(r, m)$  of the original (shown in Figure 4) and IAAFT surrogate data calculated for the different embedding dimensions of (a)  $m = 2$ , (b)  $m = 3$ , (c)  $m = 4$ , (d)  $m = 5$ , (e)  $m = 6$ , (f)  $m = 7$ , (g)  $m = 8$ , (h)  $m = 9$ , and (i)  $m = 10$ .

hypothesis is consistent with the pH and salt concentration dependences of PL enhancement as shown in Figure 3; that is, the PL intensity increases faster with increasing pH and NaCl concentration. These results suggest that ions in the vicinity of QDs are responsible for the PL enhancement. In particular, negative ions may play an important role by suppressing photoionization of QDs. However, further investigation is necessary in order to verify the mechanism.

The fluorescence oscillation itself is shown in Figures 2 and 4. At 29 °C, PL intensity exhibits intermittent oscillation (Figure 2b), whereas at 30 °C the fluorescence oscillation continues for about  $3 \times 10^4$  s with some variation (Figures 2c and 4). No significant change in the shape of the PL spectrum or peak shift is observed throughout. These results suggest that the QD aggregates communicate and synchronize throughout the medium with a resulting collective fluorescence oscillation. Similar oscillatory behavior and temperature dependence have been reported in a closed, unstirred BZ system where the temperature is one of the bifurcation parameters responsible for the transition to chaos in addition to the medium viscosity.<sup>38</sup> The fluorescence oscillation in the present QD–water system may also be governed by nonequilibrium dynamics, induced by the coupling of nonlinear chemical kinetics and diffusion. That is, interaction between QDs and negative ions may be responsible for the fluorescence oscillation because the concentration of anions adjacent to the QDs would affect the emission efficiency. Moreover, no oscillation was observed for the as-prepared nonaggregated QD suspension at temperatures in the range  $25 \leq T \leq 35$  °C. This result supports the hypothesis and suggests that the fluorescence oscillation occurs only in the presence of QD aggregates.

In most reaction–diffusion systems, temperature is one of the controlling parameters, because both reaction rate constant and diffusion coefficient are usually temperature dependent. All our understanding to date indicates that oscillatory responses occur across finite ranges of experimental conditions and the ranges depend on the system. Of course, these ranges can be narrow. In the present QD–water system, a key reaction would be photoionization of QDs that can be driven thermally and/or through the Auger process.<sup>7</sup> Since the excitation intensity is weak in our experiments ( $12 \mu\text{W}/\text{cm}^2$ ), thermally driven ionization may be dominant. Hence the QD–water system may exhibit temperature-sensitive oscillatory behavior.

Additionally, we have investigated the dependences of QD size on the PL enhancement and oscillatory behavior to validate the aforementioned interpretation. Figure 5 shows the temporal variations of normalized PL intensity of small and large MUA-capped CdSe/ZnS core/shell QDs (samples 6 and 7, respectively, in Table 1) as a function of excitation time at 30 °C. The PL intensity of small QDs enhances faster than large QDs as shown in Figure 5. In addition, large QDs also exhibit oscillatory, though weak, behavior in the PL intensity. These size-dependent features might be due to the difference in the ionizability.<sup>39</sup> We have also found that thicker capping layers suppress both PL enhancement and oscillation.<sup>40</sup> The results of the present experiments and of previous studies<sup>35–37</sup> suggest that the PL oscillation and enhancement occur only in the presence of aggregates.

The composition of the oscillation at 30 °C was determined using the magnitude of the continuous wavelet transform  $|\Psi_{a,b}|^2$  as a scalogram. A plot of the scalogram with time on the horizontal axis and frequency (converted from scale parameter

a) on the vertical axis is shown in Figure 6 for the time series data in Figure 4. The sampling interval for the raw data was 2 s, and the number of sampling points was  $N = 16\,000$ . For wavelet analysis, the data were filtered by a nonlinear noise reduction algorithm<sup>41</sup> and thinned down to  $N = 1600$  ( $\Delta t = 20$  s) by resampling. When first excited ( $t < 7700$  s), a fundamental oscillation at frequency  $\omega = 4 \times 10^{-3}$  Hz is observed. However, another peak appears after  $t \approx 7700$  s, with a frequency corresponding to the 1/2-subharmonic of the fundamental ( $\omega = 2 \times 10^{-3}$  Hz). This result suggests transient period doubling.

Figure 7 shows the correlation sums and correlation dimensions of the time series in Figure 4 for different embedding dimensions ( $2 \leq m \leq 10$ ). The raw data were preprocessed by a nonlinear noise reduction algorithm,<sup>41</sup> and the linear trend was removed. The time delay of  $\tau = 150$  s for the delay vectors was determined by the mutual information method.<sup>42</sup> Although the correlation dimension  $D_2$  does not clearly plateau over a wide range of length scales and for all embedding dimensions as shown in Figure 7b,  $D_2$  seems to converge on a certain finite value between 3 and 5.

Thus far we have established the possibility of the onset of chaos in the form of transient period doubling. The presence of a nonlinear governing dynamic of fluorescence intensity can then be examined using a plot of the correlation dimensions  $D_2$  of the original (Figure 4) and surrogate data calculated for the different embedding dimensions ( $2 \leq m \leq 10$ ), as shown in Figure 8. The correlation dimensions of all surrogates are clearly distinct from that of the original data above  $m = 6$ . Thus, the null hypothesis can be rejected and the time series can be concluded to be measurably nonlinear. Hence, the fluorescence oscillation observed in the present QD–water system may be governed by nonlinear dynamics.

## 5. Conclusion

The photoinduced fluorescence oscillation observed in a water dispersion of CdSe/ZnS core/shell quantum dots (QDs) capped with mercaptocarboxylic acid under continuous excitation was analyzed. The oscillation was found to be temperature-sensitive and to emerge in a narrow temperature range of 29–30 °C. The results of the present experiments also suggest that the fluorescence oscillation occurs only in the presence of QD aggregates. The oscillation properties such as frequency and amplitude were found to be influenced by pH, ionic species, and QD size. The oscillatory behavior was characterized by wavelet and nonlinear time-series analyses, which revealed the onset of chaos in the form of transient period doubling. Surrogate analysis verified that the governing dynamics underlying the QD–water system is probably nonlinear, suggesting that the fluorescence oscillation is a special class of photoinduced chemical oscillation. The authors intend in the future to clarify the nonlinear photochemical kinetics responsible for the collective fluorescence oscillation and to apply this phenomenon in chemical and/or biological sensors based on nonlinear dynamics.

**Acknowledgment.** This work was supported by the “University Start-Ups Creation Support System” of the Ministry of Education, Culture, Sports, Science and Technology, Japan (MEXT) and from the “Nanotechnology Materials Program—Nanotechnology Particle Project” of the New Energy and Industrial Technology Development Organization (NEDO) based on funds provided by the Ministry of Economy, Trade and Industry, Japan (METI).

## References and Notes

- (1) (a) Murray, C. B.; Norris, D. J.; Bawendi, M. G. *J. Am. Chem. Soc.* **1993**, *115*, 8706. (b) Manna, L.; Scher, E. C.; Alivisatos, A. P. *J. Am. Chem. Soc.* **2000**, *122*, 12700.
- (2) (a) Mattoussi, H.; Radzilowski, L. H.; Dabbousi, B. O.; Thomas, E. L.; Bawendi, M. G.; Rubner, M. F. *J. Appl. Phys.* **1998**, *83*, 7965. (b) Empedocles, S. A.; Neuhauser, R.; Shimizu, K.; Bawendi, M. G. *Adv. Mater.* **1999**, *11*, 1243.
- (3) (a) Takagawara, T.; Takeda, K. *Phys. Rev. B* **1992**, *46*, 15578. (b) Johnston-Halperin, E.; Awschalom, D. D.; Crooker, S. A.; Efros, A. L.; Rosen, M.; Peng, X.; Alivisatos, A. P. *Phys. Rev. B* **2001**, *63*, 205309.
- (4) Michalet, X.; Pinaud, F.; Lacoste, T. D.; Dahan, M.; Bruchez, M. P.; Alivisatos, A. P.; Weiss, S. *Single Mol.* **2001**, *2*, 261.
- (5) Goldman, E. R.; Anderson, G. P. P.; Tran, T.; Mattoussi, H.; Charles, P. T.; Mauro, J. M. *Anal. Chem.* **2002**, *74*, 841.
- (6) Chan, W. C.; Maxwell, D. J.; Gao, X.; Bailey, R. E.; Han, M.; Nie, S. *Curr. Opin. Biotechnol.* **2002**, *13*, 40.
- (7) Neuhauser, R. G.; Shimizu, K. T.; Woo, W. K.; Empedocles, S. A.; Bawendi, M. G. *Phys. Rev. Lett.* **2000**, *85*, 3301.
- (8) Gerion, D.; Pinaud, F.; Williams, S. C.; Parak, W. J.; Zanchet, D.; Weiss, S.; Alivisatos, A. P. *J. Phys. Chem. B* **2001**, *105*, 8861.
- (9) Scott, S. K. *Oscillations, Waves and Chaos in Chemical Kinetics*; Oxford University Press: Oxford, 1994.
- (10) Cross, M. C.; Hohenberg, P. C. *Rev. Mod. Phys.* **1993**, *65*, 851.
- (11) Zhabotinsky, A. M. *Chaos* **1991**, *1*, 379.
- (12) Ruoff, P.; Noyes, R. J. *J. Phys. Chem.* **1993**, *97*, 6405.
- (13) Wang, J.; Sørensen, P. G.; Hynne, F. J. *J. Phys. Chem.* **1994**, *98*, 725.
- (14) Masia, M.; Bastianoni, S.; Rustici, M. *Phys. Chem. Chem. Phys.* **2001**, *3*, 5516.
- (15) Busse, H.; Hess, B. *Nature* **1973**, *244*, 203.
- (16) Dulos, E.; DeKepper, P. *Biophys. Chem.* **1983**, *18*, 211.
- (17) Kuhnert, L. *Nature* **1986**, *319*, 393.
- (18) Kuhnert, L.; Agladze, K. I.; Krinsky, V. I. *Nature* **1989**, *337*, 244.
- (19) Rábai, G.; Hanazaki, I. *J. Am. Chem. Soc.* **1997**, *119*, 1458.
- (20) Okazaki, N.; Hanazaki, I. *J. Chem. Phys.* **1998**, *109*, 637.
- (21) Mattoussi, H.; Mauro, J. M.; Goldman, E. R.; Anderson, G. P.; Sundar, V. C.; Mikulec, F. V.; Bawendi, M. G. *J. Am. Chem. Soc.* **2000**, *122*, 12142.
- (22) Mattoussi, H.; Mauro, J. M.; Goldman, E. R.; Green, T. M.; Anderson, G. P.; Sundar, V. C.; Bawendi, M. G. *Phys. Status Solidi B* **2001**, *224*, 277.
- (23) Kagan, C. R.; Murray, C. B.; Bawendi, M. G. *Phys. Rev. B* **1996**, *54*, 8633.
- (24) Kobayashi, M. *Nonlinear Anal.* **2001**, *47*, 1749.
- (25) Chui, C. K. *An Introduction to wavelets*; Academic Press: Orlando, 1992.
- (26) Hayashi, Y.; Ogawa, S.; Cho, H.; Takemoto, M. *NDT & E Int.* **1999**, *32*, 21.
- (27) Eckmann, J.-P.; Ruelle, D. *Rev. Mod. Phys.* **1985**, *57*, 617.
- (28) Grassberger, P.; Procaccia, I. *Physica D* **1983**, *9*, 189.
- (29) Theiler, J.; Eubank, S.; Longtin, A.; Galdrikian, B.; Farmer, J. D. *Physica D* **1992**, *58*, 77.
- (30) Rapp, P. E.; Albano, A. M.; Schmäh, T. I.; Farwell, L. A. *Phys. Rev. B* **1993**, *47*, 2289.
- (31) Theiler, J.; Prichard, D. *Physica D* **1996**, *94*, 221.
- (32) Schreiber, T.; Schmitz, A. *Phys. Rev. Lett.* **1996**, *77*, 635.
- (33) The TISEAN package was used to generate surrogate data (Hegger, R.; Kantz, H.; Schreiber, T. *Chaos* **1999**, *9*, 413; Schreiber, T.; Schmitz, A. *Physica D* **2000**, *142*, 346).
- (34) Cordero, S. R.; Carson, P. J.; Estabrook, R. A.; Strouse, G. F.; Buratto, S. K. *J. Phys. Chem. B* **2000**, *104*, 12137.
- (35) Maenosono, S.; Dushkin, C. D.; Saita, S.; Yamaguchi, Y. *Jpn. J. Appl. Phys.* **2000**, *39*, 4006.
- (36) Maenosono, S.; Ozaki, E.; Yoshie, K.; Yamaguchi, Y. *Jpn. J. Appl. Phys.* **2001**, *40*, L638.
- (37) Kimura, J.; Maenosono, S.; Yamaguchi, Y. *Nanotechnology* **2003**, *14*, 69.
- (38) Masia, M.; Marchettini, N.; Zambrano, V.; Rustici, M. *Chem. Phys. Lett.* **2001**, *341*, 285.
- (39) Islam, M. A.; Herman, I. P. *Appl. Phys. Lett.* **2002**, *80*, 3823.
- (40) Eiha, N.; Maenosono, S.; Hanaki, K.; Yamamoto, K.; Yamaguchi, Y. *Jpn. J. Appl. Phys.*, to be published.
- (41) Schreiber, T. *Phys. Rev. E* **1993**, *47*, 2401.
- (42) Fraser, A. M.; Swinney, H. L. *Phys. Rev. A* **1986**, *33*, 1134.